Kinematic Analysis of a Variable-Amplitude Vibrating Screen and the Behaviour of Mixed Sea Buckthorn Particles on the Screen

Jingming Hu , Mei Yang , Qianglin Zhang , Jinfa Yang , Wuyun Zhao * , Yang Bi

Posted Date: 25 May 2026

doi: 10.20944/preprints202605.1586.v1

Keywords: variable-amplitude vibrating screen; kinematic simulation; discrete element method; RecurDyn-EDEM

 doi:10.20944/preprints202605.1586.v1

Article

Kinematic Analysis of a Variable-Amplitude Vibrating Screen and the Behaviour of Mixed Sea Buckthorn Particles on the Screen

Jingming Hu [1], Mei Yang [1], Qianglin Zhang [1], Jinfa Yang [1], Wuyun Zhao [1,*] and Yang Bi [2]

[1] College of Mechanical and Electrical Engineering, Gansu Agricultural University, Lanzhou 730070, PR China

[2] College of Food Science and Engineering, Gansu Agricultural University, Lanzhou 730070, PR China

* Correspondence: zhaowy@gsau.edu.cn; Tel.: 86+15101322368

Abstract

Variable amplitude vibrating screens are widely used in the screening of frozen sea buckthorn berry particles. The study of its motion characteristics and the behavior of particles on the screen surface is crucial to optimize the screening process and improve the performance and screening efficiency of the equipment. In this study, the variable amplitude vibrating screen is taken as the research object, its structural composition and working principle are described, and the kinematic simulation of the variable amplitude vibrating screen is carried out by using RecurDyn. The results show that the amplitude and speed of the screen surface in the vertical direction gradually increase from the feed end to the discharge end, which helps the particles to pass through the screen surface quickly; the horizontal speed of the screen surface remains consistent in each section. The crank length affects the amplitude of the screen surface, while the crank speed determines the vibration frequency of the screen surface. By using EDEM and RecurDyn software, the dynamics model of the particles and the sieve surface was established, and the two-way coupling of the discrete element model was realized. The coupled simulation results show that the dynamic sieving efficiency increases with the increase of crank length and rotational speed. The dynamic sieving efficiency reaches the highest when the crank length is 20 mm and the rotational speed is 208 r/min. The crank length and rotational speed have a significant effect on the thickness of the particle layer on the screen surface and the number of particles passing through the screen: the thicker the particle layer is, the longer the particles stay on the screen surface; the accuracy of the model is verified by field experiments, and the results show that the coupled simulation model is basically in line with the field test data. The influence of crank length and rotational speed is crucial in the study of variable amplitude vibrating screen. The study of the motion characteristics of the variable amplitude vibrating screen and the behavior of the particles on the screen surface can provide a theoretical basis for the efficient operation and optimal design of the variable amplitude vibrating screen.

Keywords: variable-amplitude vibrating screen; kinematic simulation; discrete element method; RecurDyn-EDEM

1. Introduction

The screening of materials is a crucial step in particle classification [1–3]. Variable-amplitude vibrating screens, which exhibit a gradual change in amplitude from the feed end to the discharge end, are widely used in large-scale mineral processing and agricultural harvesting machinery for the separation of granular materials. This amplitude variation enhances the processing capacity of the screen surface [4–6].

Numerous scholars have conducted extensive research on particle stratification, sieving, and flow on vibrating screens using physical experiments and mathematical models. These studies have

 doi:10.20944/preprints202605.1586.v1

revealed the motion trajectories of vibrating screen surfaces and the behavior of particles under different motion conditions [7–12].

Jiang et al. utilized theoretical analysis and ADAMS dynamics software to perform dynamic simulation analysis of vibrating screen motion characteristics, uncovering the collision mechanism between particles and the screen surface [13]. Wang et al. employed dynamic simulation software to conduct kinematic analysis of bionic sieve surfaces, obtaining the relationship between velocity, displacement, and time for each sieve surface [14]. Guo et al. investigated the displacement and velocity of the center of mass of a combined vibrating screen using multibody dynamics (MBD) software. They found that varying frequency and amplitude combinations could alter particle motion states, facilitating the loosening and stratification of wet particles [15]. Wang et al. derived a mathematical model for the motion of a reciprocating vibrating screen using the matrix method and performed numerical simulations and analysis in MATLAB. Their results indicated that the motion trajectories of the screen surface varied at different positions [16]. Cundall et al. proposed a discrete element-based numerical simulation method capable of simulating complex particle motion behaviors [17]. Elskamp et al. optimized sieving process parameters using the discrete element method (DEM), demonstrating that operating parameters and particle shape significantly influence sieving efficiency [18].Ning et al. studied the fundamental principles of the sieving process on oscillating screens using EDEM, analyzing the effects of different vibration parameters on particle stratification and sieving [19]. Ma et al. simulated the motion of seeds and stalks on the reciprocating vibrating screen of a combine harvester using EDEM software. They observed that the reciprocating motion caused particles at the feed end to move rapidly backward, hindering material separation [20]. Li et al. employed the discrete element method to study the sieving process of wet particles on multi-deck vibrating screens, identifying optimal parameters for vibration frequency, amplitude, and screen inclination [21].Delaney et al. investigated the shape and flow rate of particles on vibrating screens, concluding that modeling particles as non-spherical entities more accurately represents their actual flow behavior [22]. The bidirectional coupling of multibody dynamics and discrete element methods offers a novel approach to studying interactions between complex mechanisms and particles, and has been widely applied in particle and machinery research [23–25]. Wu et al. conducted research on the bidirectional coupling of discrete elements and multibody dynamics for particle-screen surface interactions, achieving bidirectional coupling between flexible plates and particles [26]. For variable-amplitude vibrating screens, understanding the dynamic characteristics of the screen surface under different motion conditions and the behavior of particles with varying sizes is essential for optimizing screen design and improving sieving performance [6,27–29].

Although there have been studies on the dynamics of variable-amplitude vibrating screens and the motion behavior of particles on the screen surface, research on the sieving of mixed particles of sea buckthorn frozen berries using variable-amplitude vibrating screens remains limited. This study aims to establish a mathematical model of the variable-amplitude vibrating screen mechanism through theoretical analysis. Using RecurDyn software, the motion characteristics of the screen surface at different positions under varying crank lengths and rotational speeds will be analyzed to optimize the parameter combinations of the variable-amplitude vibrating screen. Additionally, the motion behavior and sieving mechanism of mixed particles of sea buckthorn frozen berries on the screen surface will be investigated through joint simulation using RecurDyn and EDEM. The findings will provide valuable insights for the efficient operation and optimized design of variable-amplitude vibrating screens in the cleaning and selection of sea buckthorn frozen berries.

2. Composition and Working Principle of Variable-Amplitude Vibrating Screen

The variable-amplitude vibrating screen consists of an offset crank, a double rocker mechanism and a crank slider mechanism as shown in Figure 1. The variable amplitude vibrating screen generates excitation force under the high speed rotation of the crank, as a result, the materials on the screen was thrown up, stratified, sieved through the screen, and transported to the discharge port, the materials at the discharge port was separated by a fan for the second time.The offset crank slider

 doi:10.20944/preprints202605.1586.v1

mechanism is composed of DCEF, and the crank double rocker mechanism is composed of ABCEF, as shown in Figure 2.

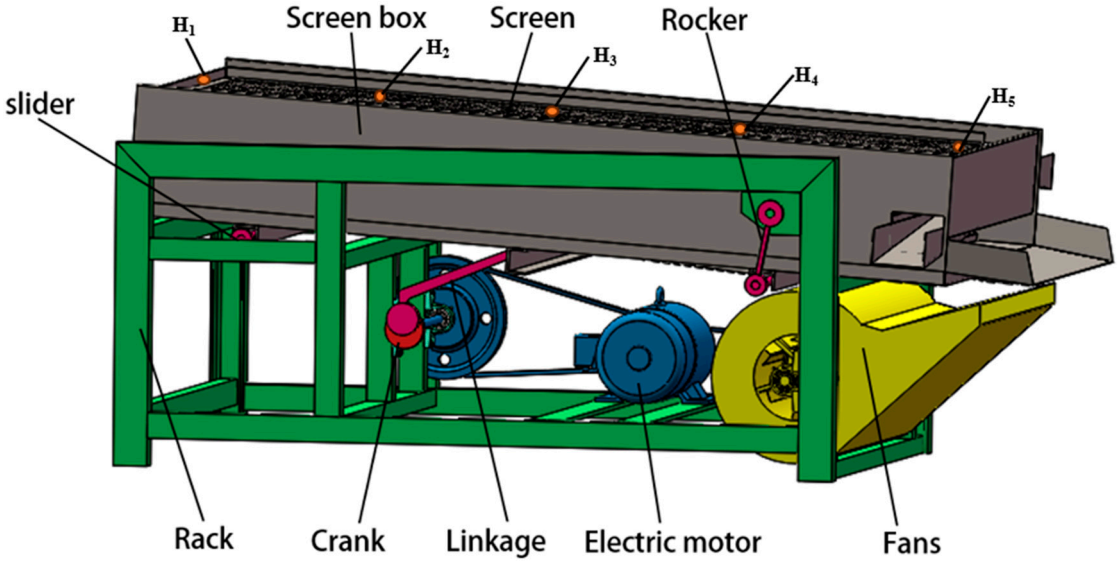

Figure 1. Variable-amplitude vibrating screen.

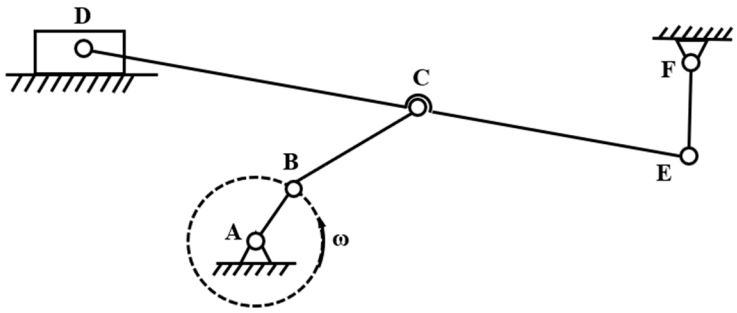

Figure 2. Mathematical model of variable-amplitude vibrating screen mechanism.

3. Materials and Methods

3.1. Motion Simulation of Variable-Amplitude Screen Based on Recurdyn

In this paper, 3D software was used to establish a 3D model of the variable-amplitude vibrating screen. The parts and structures in the model that have little influence on the simulation results were omitted, and the relatively static rigid body parts were merged into a whole by Boolean operation, to avoid the loss of information imported into the simulation model. Define materials in Material Type for each part of the imported model, add rotating pairs to the rotating parts [30], and add moving pairs to the sliding parts of the frame and screen box. The connection relationship between components of the variable-amplitude vibrating screen are shown in Table 1.

Table 1. Variable-amplitude vibrating screen components connection relationship.

Constraint number	Constraint object	Constraint type
1	Rack-ground	Fix pair
2	Crank-shaft	Revolute pair
3	Linkage-crank	Revolute pair
4	Linkage-rack	Revolute pair
5	Rocker-rack	Revolute pair
6	Rocker-screen box	Revolute pair

 doi:10.20944/preprints202605.1586.v1

7	Slider-rack	Revolute pair
8	Slider-screen box	Translate pair

3.2. EDEM-Recurdyn Coupling Simulation

3.2.1. Particle Contact Model

This study selected the Hertz-Mindlin contact model, which was proposed by Mindlin and Deresiewicz in 1953 [31]. There are damping forces in the normal force and tangential force in the model, and the damping coefficient is related to the recovery coefficient [32], the friction force satisfies Coulomb's theorem (Cundall and Strack 1979) [18].

The normal force F_n in the model is a function of the normal overlap δ_n, and is calculated by the following equation:

$$F_n = \frac{4}{3} E^* \sqrt{R^*} \delta_n^{\frac{3}{2}} \tag{1}$$

$$\frac{1}{E^*} = \frac{(1-\vartheta_i{}^2)}{E_i} + \frac{(1-\vartheta_j{}^2)}{E_j} \tag{2}$$

$$\frac{1}{R^*} = \frac{1}{R_i} + \frac{1}{R_j} \tag{3}$$

where E^* is the equivalent Young's modulus, R^* is the equivalent radius, δ_n is the normal overlap amount, E_i and E_j are the Young's modulus of particles i and j, ϑ_i and ϑ_j are the Poisson's ratio of particles i and j, R_i, and R_j are the radius of contacting particles i and j.

The damping force F_n^d in the model is calculated by the following equation:

$$F_n^d = -2\sqrt{\frac{5}{6}} \beta \sqrt{S_n M^*} V_n^{rel} \tag{4}$$

$$M^* = \left(\frac{m_i m_j}{m_i + m_j} \right) \tag{5}$$

$$\beta = \frac{-lne}{\sqrt{ln^2 e + \pi^2}} \tag{6}$$

$$S_n = 2E^* \sqrt{R^* \delta_n} \tag{7}$$

$$V_n^{rel} = (V_i - V_j) \tag{8}$$

where M^* is the equivalent mass, e is the restitution coefficient, V_n^{rel} is the normal component of relative velocity, β and S_n are the normal stiffness.

The tangential force is calculated by the following formula:

$$F_t = -S_t \delta_t \tag{9}$$

$$S_t = 8G^* \sqrt{R^* \delta_n} \tag{10}$$

 doi:10.20944/preprints202605.1586.v1

$$G^* = \frac{2-{\sigma_i}^2}{G_i} + \frac{2-{\sigma_j}^2}{G_j} \tag{11}$$

where G^* is the equivalent shear modulus, G_i and G_j are the equivalent shear modulus of particles i and j, respectively.

The tangential damping force F_t^d is calculated by the following equation:

$$F_t^d = -2\sqrt{\frac{5}{6}}\beta\sqrt{S_t m^*}V_t^{rel} \tag{12}$$

where V_t^{rel} is the relative tangential velocity.

3.2.2. Particle Model

The application of EDEM software to establish an accurate material model is the basis for ensuring the validity of the simulation results [33,34], in this study, frozen sea buckthorn branch-fruits were selected to be separated and processed by the fruit removal machine to obtain the frozen berries and branch materials, which mainly contain spherical particles of frozen berries, non-spherical twigs, fruit stems and other impurities. The Hertz-Mindlin particle contact model was used for simulation in EDEM software simulation [35] and the mechanical properties of each material and the contact properties between each material are shown in Tables 3 and 4.

Table 3. Mechanical properties of materials.

Materials	Poisson's ratio	Shear modulus /MPa	Density/(kg/m³)
Frozen berry	0.41	2.79	1.07×10^3
Branch	0.50	3.43	0.93×10^3
Fruiting stem	0.43	7.22	0.22×10^3
Screen surface	0.29	2.05×10^5	7.93×10^3

Table 4. Interaction properties of materials.

Parameters	Collision recovery coefficient	Static friction factor	Rolling friction factor
Branchesand branches	0.483	0.266	0.031
Branches and frozen berries	0.584	0.266	0.041
Branches and fruit stems	0.543	0.316	0.031
Branches and screen surfaces	0.268	0.373	0.065
Frozen berries and frozen berries	0.584	0.316	0.076
Frozen berries and stems	0.483	0.266	0.031
Frozen berries screen surface	0.242	0.212	0.023
Fruit stems and fruit stems	0.44	0.322	0.075
Fruit stem and screen surface	0.259	0.436	0.075

After quick-frozen sea buckthorn branches and fruits were mechanically removed in the workshop environment of -5℃-8℃, the mixed particles of sea buckthorn fall down to the conveyor belt, and the particles were transferred to the feed end of the screen surface through the conveyor belt. The mixed particles on the screen were statistically analyzed, to obtain frozen sea buckthorn berries, the proportion of sea buckthorn frozen berries, branches and fruit stems was 67%, 7% and 26%.

In EDEM, sea buckthorn frozen berries were modeled using a single sphere, and the rest of the materials were modeled using the multi-sphere overlapping method, as shown in Figure 3 [36]. It is difficult to simulate the motion of complex models in EDEM, in order to make the simulated variable-

 doi:10.20944/preprints202605.1586.v1

amplitude vibrating screen consistent with the motion of the variable-amplitude vibrating screen in production, EDEM-Recurdyn was used for coupled simulation. according to the experiments in Table 2, the motion behavior of mixed particles on the screen surface under different crank lengths and speeds was studied. The geometric parameters and operating parameters of the variable-amplitude vibrating screen are shown in Table 5, the variable-amplitude vibrating screen is composed of three layers of screens, the diameter of the first layer of screen holes was 12 mm and the hole spacing was 16 mm, the hole diameter of the second layer was 8 mm, and the hole spacing was 11 mm, the diameter of the third layer screen was 5 mm, it was composed of a round hole screen with a hole spacing of 6mm, the spherical particles were composed of frozen berry particles, and the non-spherical particles were composed of frozen branches and fruit stems.

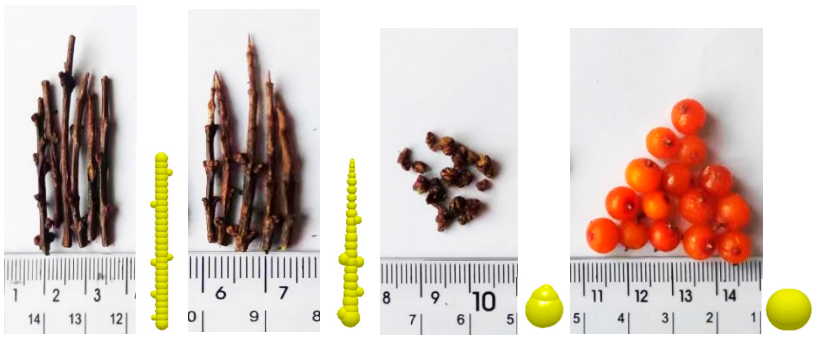

Figure 3. Sea buckthorn branches, fruit stems, frozen berries and models.

Table 5. Material properties of particles and screen used in the simulations.

Parameter	Value
Screen length (mm)	1800
Screen width (mm)	990
screen aperture (mm)	12, 8, 5, Round holes
Screen angle	3°～8°
Linkage l_2, l_3 (mm)	35, 1225
Rocker l_4 (mm)	170
Conveyor movement speed (m/s)	0.5
Particle feeding amount (kg)	3
Frozen berry particle (mm)	5.6
Columnar branch particles (mm)	42×2 (Length×diameter)
Conical branch particles (mm)	38×1.8 (Length×diameter)
Fruit stem particles (mm)	3×3.5×2.7 (Length×wide×height)

3.2.3. Evaluation Method

In industrial production, screening efficiency is often used to evaluate the screening performance of vibrating screens.[37–39] Screening efficiency refers to the ratio of the mass of fine particles that pass through the sieve during the screening process (actual screening mass) to the mass of particles smaller than the sieve hole diameter in the feed particles, the formula is shown in 13:

$$\delta = \left(\frac{m_{p1}}{m_{p2}} - \frac{m_{d1}}{m_{d2}} \right) \times 100\% \quad (13)$$

where δ is the screening efficiency, m_{p1} is the particles with a diameter smaller than the diameter of the sieve hole, m_{p2} is the total mass of particles with a diameter smaller than the diameter of the sieve holes, m_{d1} is the mass of particles with a diameter larger than the diameter of the sieve hole that passes through the sieve holes, and m_{d2} is the total mass of particles with a diameter larger than the diameter of the sieve hole.

 doi:10.20944/preprints202605.1586.v1

In the EDEM simulation, approximately spherical particles which larger than diameter of the sieve hole of the third layer, and the mass passing through the sieve was negligible, during the simulation process, the sieving of particles is a dynamic process, this paper introduced dynamic screening efficiency method to study the changes in screening efficiency, for dynamic changes in simulation time, Formula 26 was simplified into a dynamic screening efficiency calculation formula, such as Formula 14:

$$\delta_t = \frac{m_{pt1}}{m_{pt2}} \tag{14}$$

where δ_t is the sieving efficiency at time t, m_{pt1} 1 is the screened particles smaller than the hole diamter of screen aperture at time t, and m_{pt2} is the total mass of particles with diameters smaller than the hole diamter of screen at time t.

4. Results and Discussion

4.1. Simulation Analysis of Screen Surface Displacemen

Figures 4 and 5 show the change rule of displacement with time at different positions in the Y and X directions of the variable-amplitude vibrating screen under different crank lengths and rotational speeds, the displacement curves of the X and Y axes were roughly sinusoidal.

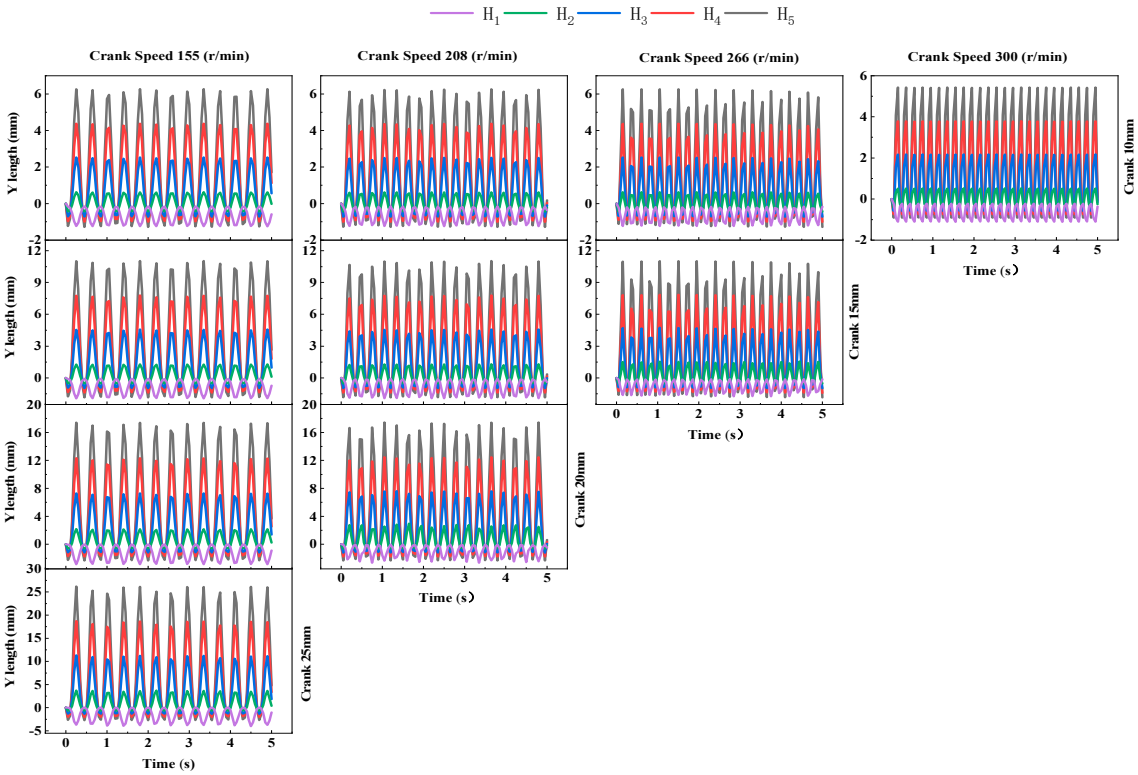

Figure 4. Y-direction displacement diagram of variable-amplitude vibrating screen.

As shown in Figure 4 the displacement of the sieve surface along the Y-direction increases sequentially from point H_1 to H_5, and when the crank length was 10 mm and the rotational speed was 155 r/min, the maximum moving distance at each point from H_1 to H_5 was 0.86 mm, 0.93 mm, 2.75 mm, 4.54 mm, 6.34 mm, respectively, which was conducive to the rapid movement of the impurity particles on the sieve surface towards the backward, and accelerate the separation of the impurity particles from seabuckthorn frozen berries [4]. Under different crank lengths, the crank speed cannot change the amplitude of the screen surface at each point, the larger the crank speed the shorter the time for the screen surface displacement to reach the peak value. At different crank speeds, the displacement in the Y direction at each point on the screen surface increased with the increase of

 doi:10.20944/preprints202605.1586.v1

crank length, when the crank speed was 155 r/min, the displacement at point H_1 was 6.34 mm, 12.86 mm, 19.73 mm and 28.96 mm for crank lengths of 10 mm, 15 mm, 20 mm and 25 mm, respectively.

As shown in Figure 2 due to the horizontal displacement of the variable-amplitude vibrating screen is controlled by the offset crank-slider mechanism, the horizontal displacement of each point on the screen surface is kept the same. As shown in Figure 5 the displacement of the screen surface in X direction increased with the increase of crank length, when the crank speed was 155 r/min, corresponding to crank lengths of 10 mm, 15 mm, 20 mm and 25 mm, the displacement in X direction were 26.45 mm, 40.95 mm, 56.74 mm, 74.47 mm. The displacement of the screen surface in the X-direction remained constant with increasing crank speed for different crank lengths, and when the crank was 10 mm, the speeds of 155 r/min, 208 r/min, 266 r/min and 300 r/min corresponded to the displacement in X direction oscillates around 20 mm.

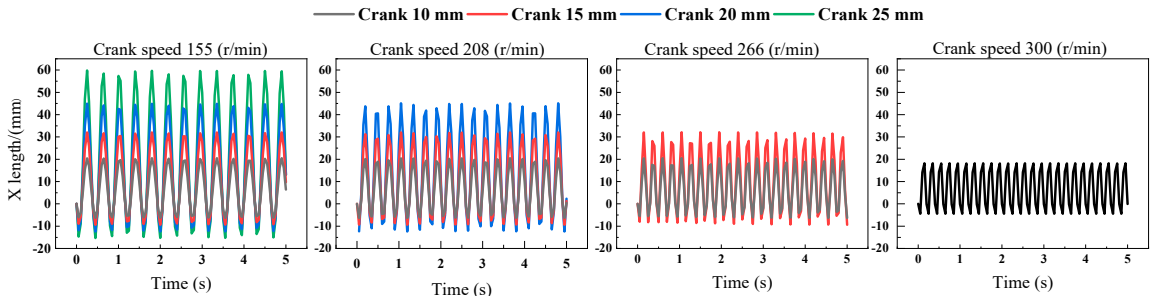

Figure 5. X-direction displacement diagram of variable-amplitude vibrating screen.

4.2. Simulation Analysis of Sieve Surface Velocity

Figures 6 and 7 show the velocity diagrams of the screen surface in X and Y directions for variable-amplitude vibrating screen at different crank lengths and speed. A total of 512 points were collected from the velocity map at different points on the sieve surface [14], the velocity map was rapidly changed by Fourier to obtain the relative frequency and amplitude characteristics of thevelocity in the X and Y directions, As shown in Figures 8 and 9.

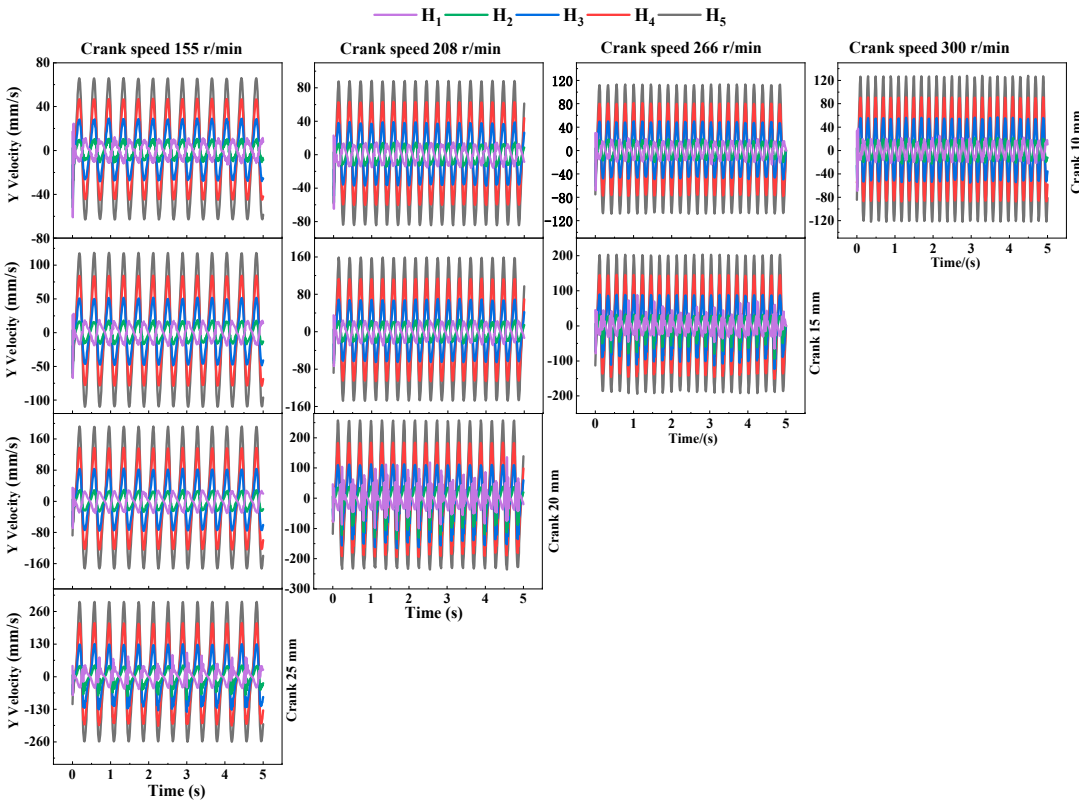

 doi:10.20944/preprints202605.1586.v1

Figure 6. Y-Direction Velocity Diagram of Variable-Amplitude Vibrating Screen.

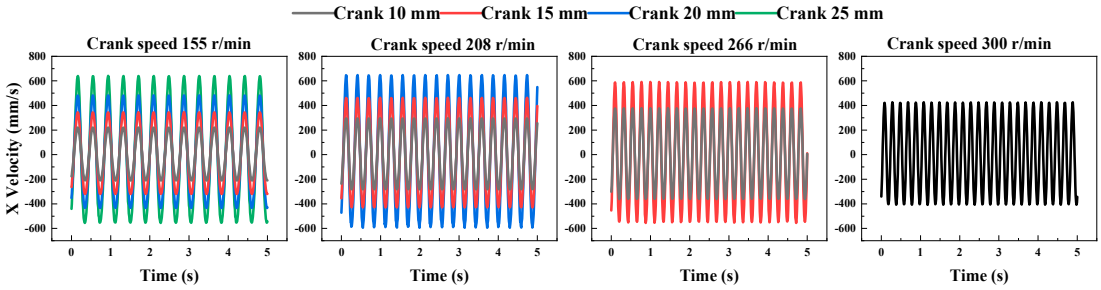

Figure 7. Velocity diagram of variable-amplitude vibrating screen in X direction.

As shown in Figures 6 and 7, the velocities in the X and Y directions of the variable-amplitude vibrating screen exhibit an approximate sinusoidal distribution. The velocities at various points on the screen surface in the Y and X directions increase with increasing crank length and rotational speed, respectively. The velocities along the Y direction for points H1 to H5 on the screen surface increase sequentially.

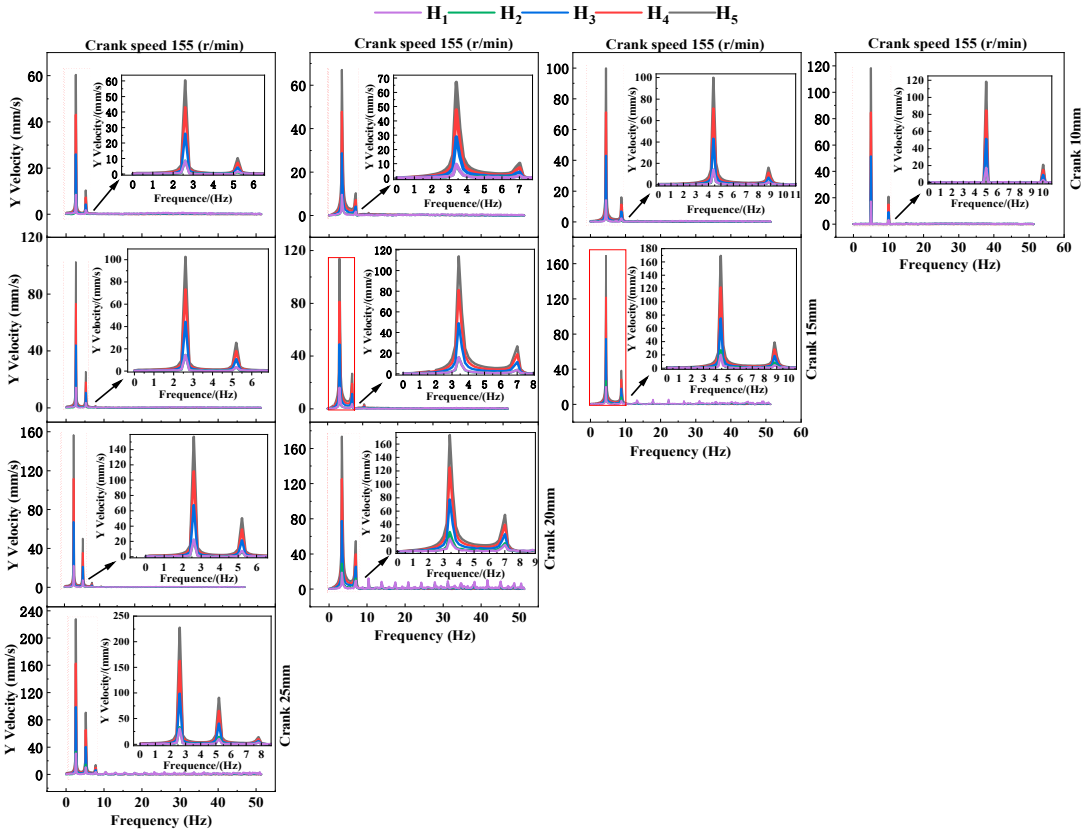

Figure 8. Amplitude versus frequency characteristics of the Y-direction velocity of the variable-amplitude vibrating screen.

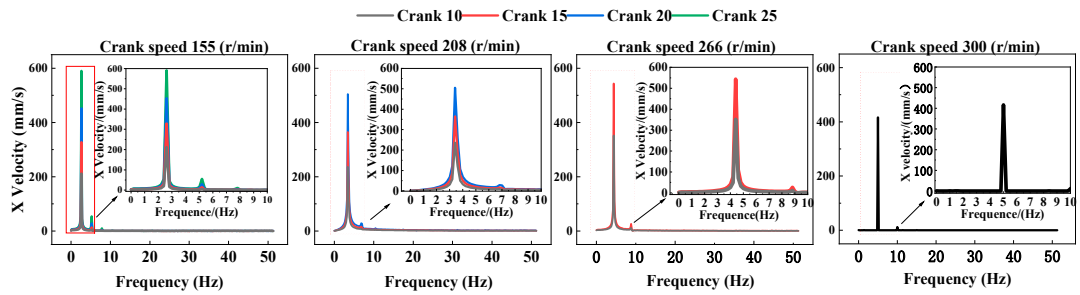

 doi:10.20944/preprints202605.1586.v1

Figure 9. Frequency and amplitude plots of X-direction velocity of variable-amplitude vibrating screen.

Figures 8 and 9 show the amplitude and relative frequency variation characteristics of the screen surface velocity in the Y direction and X direction of the variable-amplitude vibrating screen, the relative frequency of the screen surface speed of the variable-amplitude vibrating screen was related to the crank speed and was independent of crank length. Due to the low damping of the variable-amplitude vibrating screen system, the initial response of the variable-amplitude screen and the accompanying free vibration persists, led to the appearance of another frequency component in the frequency plot of velocity. When the crank speed was 155 r/min, 208 r/min, 266 r/min, 300 r/min, the corresponding main frequency was 2.6 Hz, 3.4 Hz, 4.4 Hz, 5.0 Hz [11]. When the crank speed and length exceeding a certain value, the relative frequencies of multiple high frequencies appeared at the velocity of the variable-amplitude vibrating screen in the Y direction, which will destroy the stability of the screen surface of the amplitude-vibrating screen, resulting in the failure of the amplitude-vibrating screen to work properly.

4.3. Numerical Study of Screening Process

During the simulation process, in order to maintain the consistency of the motion state of the simulated mixed particles and the particles in production, the mixed particles were dropped to the conveyor belt during the simulation process and the particles were sent to the feed end of the variable-amplitude vibrating screen through the conveyor belt, when falling to the screen surface, the mass of the mixed particles increased first and then decreased, and finally all falled into the feed end, subsequently the mixed particles were stratified and sereened under the action of the variable-amplitude vibrating screen, pass through the sieve, and finally separated the mixed particles. Figure 10 shows the screening process of mixed particles on the variable-amplitude vibrating screen when the crank length was 20 mm and the rotation speed was 266 r/min. Figure 10a shows that the mixed particles fell to the screen surface at 2.5 s, and some particles were stratified. Figure 10b shows that after 3.5 s, a large amount of material fell into the first layer of screen and was thrown up under the action of the vibrating screen, the material collided with the screen surface, and particles smaller than the screen aperture passed through the screen, and the particles were stratified. Figure 10c shows that the upper layer material was basically screened at 4.5 s, the middle layer screen shared the screening pressure of the lower layer screen, making the mixed particles looser and the separation rate of the lower layer screen particles accelerated. When the mixed particles fell into the screen, the particles on the screen move backward, and the number of collisions between the mixed particles and the screen surface increased, the stratified area of the mixed particles on the screen was mainly distributed near the feed inlet.

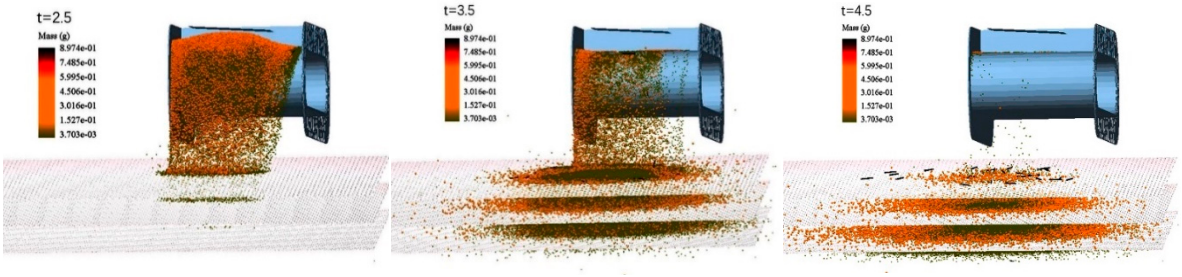

(a) t=2.5 s (b) t=3.5 s (c) t=4.5 s

Figure 10. Material simulation screening process, pictures a, b, c were colored according to particle mass (dark green to black indicate particle mass from large to small).

4.4. Analysis of Screening Effect

The number of particles passing through the sieve is an important indicator of the effectiveness of sieving [3]. Figure 11 shows the situation of spherical particles passing through the screen, the

 doi:10.20944/preprints202605.1586.v1

number of particles passing through the screen was related to the feeding amount of the material, the thickness of the screen surface, and the movement parameters of the material [11,14]. In Figure 11a, before 4.3 s, the amount of granular material passing through the first layer of sieves was greater than the amount of particles on the second layer of sieves, at 4.3 s, the number of particles on the second layer of sieves reached its peak value, after the simulation time exceeded 4.3 s, the number of materials passing through the first layer of sieves was less than the number of materials passing through the second layer of sieves, and the number of particles on the sieves gradually decreased. As shown in Figure 11b, the spherical particles on the third layer of sieve cannot pass through the sieve holes, the number of spherical particles on the sieve passing through the sieve gradually increased with the simulation time and finally stabilized. As shown in Figure 11a,b, as the crank length and rotational speed increased, the number of spherical particles passing through the first layer of the screen increased, and the increase in the thickness of the material on the second layer of the screen resulted in a decrease in the number of spherical particles passing through the screen in that layer.

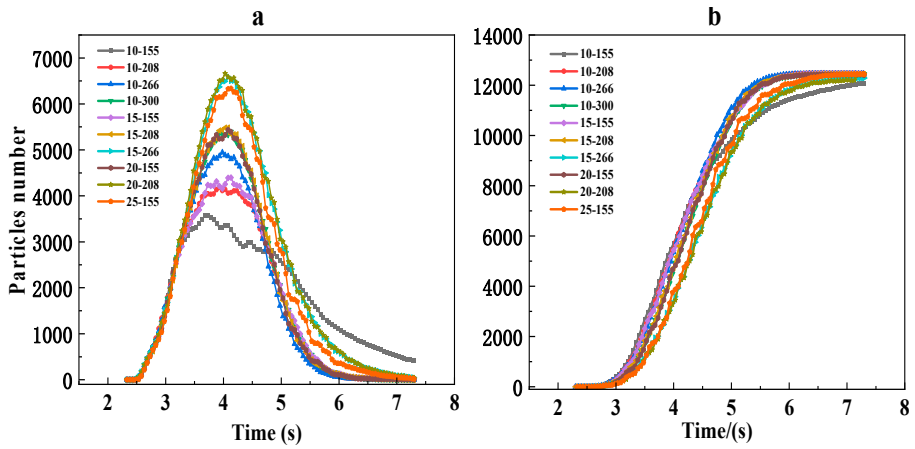

Figure 11. Number of spherical particles passing through the sieve of a variable-amplitude vibrating screen. (a) Number of frozen berries in the middle of the first two screen layers (b) Number of frozen berries in the middle of the second three screen layers.

Figure 12 shows the sieving situation of non-spherical particles, in Figure 12a, the non-spherical particles and spherical particles have the same tendency to pass through the sieve, but the peak time of non-spherical particles on the sieve is earlier than that of spherical particles, the main reason is that the particles smaller than the sieve hole in the non-spherical particles have more contact opportunities with the sieve hole, resulting in a shorter sieve penetration time than spherical particles. Figure 12b shows the changes in the number of material between the second and third screen at different crank lengths and speeds, with the increase of simulation time, the number of non-spherical particles in the material on the screen of the amplitude-vibrating screen increased and then slowly decreased, the number of non-spherical particles varies greatly with different crank lengths and speeds, the crank length is 10 mm and the speed is 155 r/min, the number of non-spherical particles passing through the sieve is much lower than that of particles passing through the sieve under the other parameters of the motion. Figure 12c shows a gradual increase in the number of non-spherical particles passing through the sieve as the crank length and rotational speed increase. As shown in Figures 11 and 12, the number of particles passing through the sieve is related to the thickness of the particles on the sieve surface; the thicker the particles on the upper sieve, the longer the particles stay on the sieve, resulting in a decrease in the number of particles passing through the sieve.

 doi:10.20944/preprints202605.1586.v1

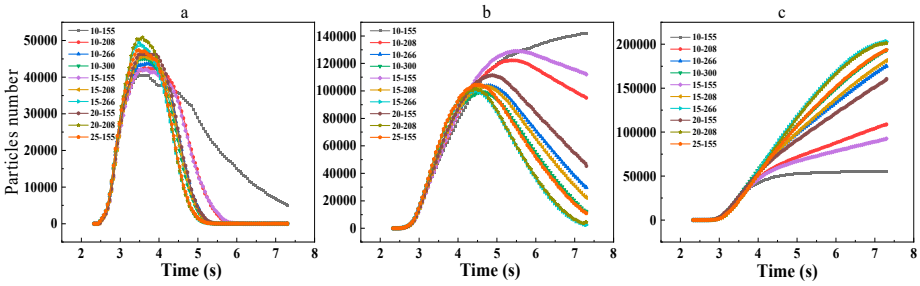

Figure 12. The number of non-spherical particles passing through the variable-amplitude vibrating screen. (a) Non-spherical impurities in the middle of the first and second screen (b) Non-spherical impurities in the middle of the second and third screen (c) Non-spherical impurities under the third screen.

Figure 13 shows the effect of different crank lengths and rotational speeds on the screening efficiency of the material, under different motion parameters, there is a large gap in the screening efficiency of variable-amplitude vibrating screens, when the simulation time is 7.3 s, the crank length is 20 mm, the rotational speed is 208 r/min, the maximum value of the screening efficiency is 98.56 %, when the crank length is 10 mm, the rotational speed is 155 r/min, the minimum screening efficiency is 25.54 %, the screening efficiency increased with the increase of crank length and rotational speed.

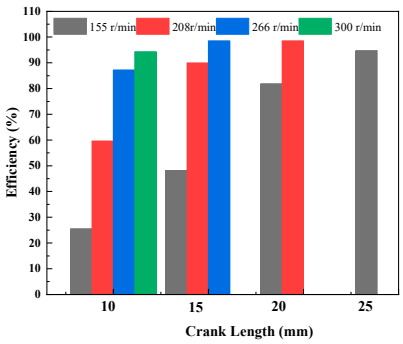

Figure 13. Screening efficiency of variable-amplitude vibrating screen at 7.3 s.

When the crank length is 15 mm, speed is 208 r/min and crank length is 20 mm, speed is 266 r/min, respectively, corresponding to the screening efficiency of 98.12 %, 98.56 %, so in order to obtain a higher screening efficiency under the conditions of ensuring the normal operation of the amplitude-vibrating screen, we should keep the crank speed and crank length matching.

4.5. Effect of Motion Parameters on Velocity

The average velocity of the particles on the variable-amplitude vibrating screen under different motion parameters is shown in Figure 14, when the particles falled from the conveyor belt to the screen surface, the potential energy of the particles is transformed into kinetic energy, and the particles obtained a high falling speed, and the velocity reached the maximum value at 2.88 s, with a value of 1.06 m/s. After the particles collided with the screen surface from 2.88 s to 3.3 s, some of the particles completed the penetration of the screen, and the rest of the particles were thrown up by the surface to move forward, and the average velocity of particles decreased rapidly, and the average velocity of the particles on the sieve first decreased and then tended to a stable value. The change of the average velocity amplitude of the particles on the sieve gradually increased and was consistent with the change of the velocity amplitude of the sieve surface. As shown in Figure 14, as the simulation time proceeds, the average velocity of the particles on the sieve gradually converged to a dynamic stability value under different motion parameters, when the crank length is 10 mm, 15 mm, 20 mm, 25 mm, the average velocity of the particles under different rotational speeds kept floating up and down at 0.15 m/s, 0.2 m/s, 0.25 m/s, 0.75 m/s, the rotational speed had no significant effect on

 doi:10.20944/preprints202605.1586.v1

the dynamic stability value of the particles on the sieve, but only affected the time for the particles to reach the peak value.

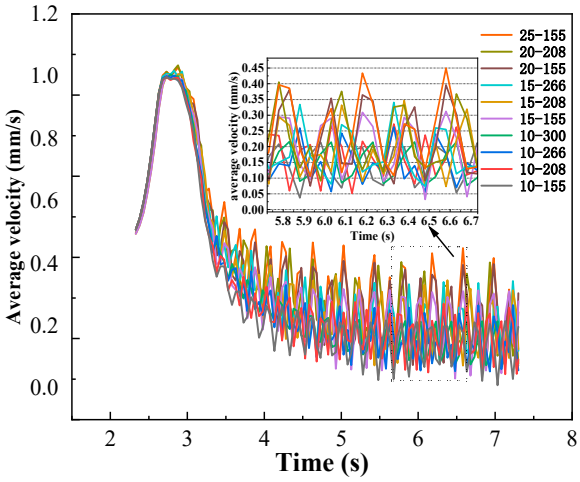

Figure 14. Average velocity of particles with different motion parameters.

4.6. Effect of Material Displacement on the Screen Surface

Figure 15 shows the average displacement of particles on each layer of screen surface under different crank lengths and rotational speeds. As shown in Figure 15a–c, the particles on the variable-amplitude vibrating screen have a tendency to move backwards, which is not favourable for the movement of the material. Due to the amplitude and speed of the screen surface along the Y-direction from the feed port to the discharge port of the amplitude-variable vibrating screen increase gradually, it can ensure that the material on the screen surface moves in the direction of the discharge port. As shown in Figure 15, when the crank length is 10 mm and the rotational speed is 155 r/min, the displacement of the particles on the three-layer screen surface is almost unchanged, and the particles cannot be quickly conveyed to the discharge port. When the simulation time is 7.3 s, the maximum value of the average displacement of the particles on the first layer of the screen surface is 637 mm, and the minimum value is 216 mm, the maximum value of the average displacement of the particles on the second layer of the screen surface is 485 mm, and the minimum value is 243 mm, and the maximum value of the average displacement of the particles on the third layer of the screen surface is 494 mm, and the minimum value is 199 mm, this shows that at different crank lengths and rotational speeds, the amplitude-vibrating screen has a greater variability of particle moving distance on the screen surface under different crank lengths and rotational speeds, and the moving distance of the particles increases with the increase of the crank length and rotational speed.

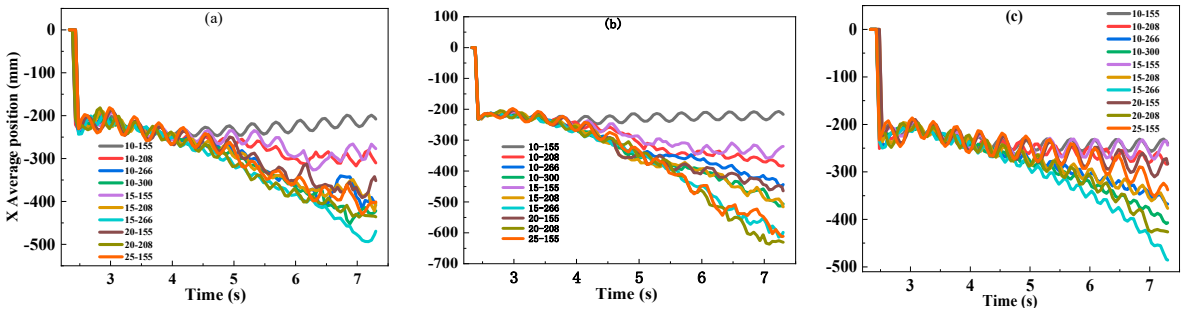

Figure 15. Mean displacement of particles in X direction on the sieve surface for different structure and motion parameters (a: particles onthe first layer of the sieve surface; b: particles on the second layer of the sieve surface;c: particles on the third sieve surface).

 doi:10.20944/preprints202605.1586.v1

4.6. Experimental Verificatio

To validate the effectiveness of the simulation model, a series of simplified field experimental were conducted. To prevent the thawing of frozen berries [40], the tests were performed in an environment maintained at -8°C. The screen parameters were consistent with those in the simulation model. Since the crank length of the amplitude-vibrating screen was not easily adjustable, it was fixed at 15 mm, while the crank speed was regulated via a frequency converter and a tachometer to 155 r/min, 208 r/min, and 266 r/min, corresponding to the simulation parameters

As shown in Figure 16, the material distribution on the screen surface during field tests closely matched the simulation results: after being fed onto the screen, the material rapidly spread toward the discharge end and both sides while simultaneously passing through the screen. Quantitative comparison in Figure 17 shows that at the crank speeds of 155 r/min, 208 r/min, and 266 r/min, the errors between the simulation and field test results were 0.68%, 1.82%, and 4.18%, respectively. These results confirm a fundamental agreement between the coupled simulation model and the experimental data.

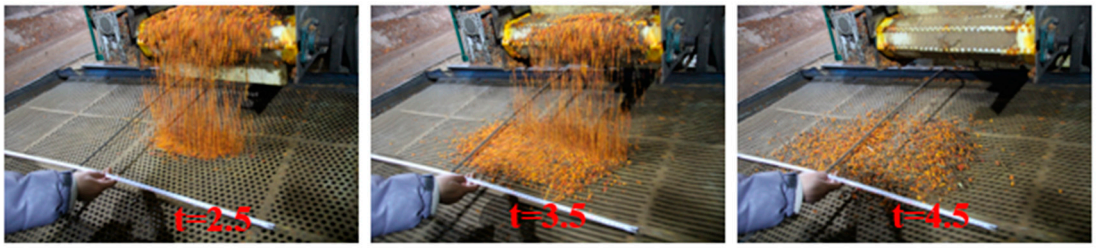

Figure 16. Experimental prototype of variable-amplitude vibrating screen.

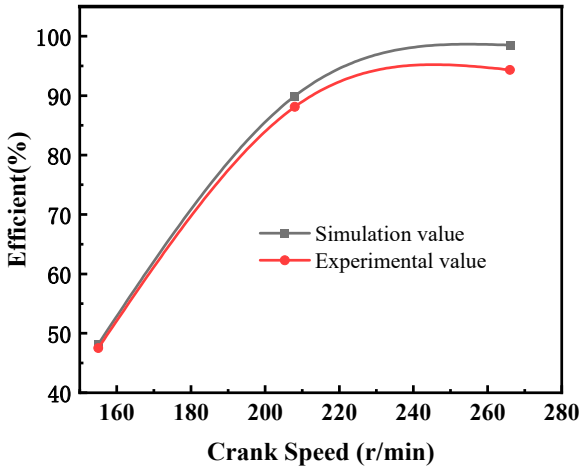

Figure 17. Field test validation results.

5. Conclusion

In this study, based on EDEM and Recurdy software, a series of numerical simulations of variable amplitude vibrating screen are carried out to study the influence of crank speed and length on the motion characteristics of different positions of the screen surface of the variable amplitude vibrating screen and the granular materials on the screen, the following conclusions are obtained:

The displacement and speed of the screen surface of variable-amplitude vibrating screen increases sequentially from the feed port to the discharge port, which is favourable to the rapid movement of sea buckthorn frozen berries, branches and other mixed particles. Crank length and rotational speed directly affect the displacement and speed of the screen surface, simulation results show that the crank length and rotational speed of the vibrating screen mechanism are limited by its

 doi:10.20944/preprints202605.1586.v1

own structure, their threshold value can not be exceeded, in order to ensure the normal operation of the amplitude-vibrating screen.

Particle passage is influenced by both particle size and material bed thickness. An increased bed thickness prolongs the residence time of particles on the screen, consequently diminishing the screening rate. This can be counteracted by optimizing the crank rotational speed and length, which facilitates prompt stratification of the material and thereby improves dynamic screening efficiency.

The cleaning process of sea buckthorn berries is complex. The accuracy of a coupled EDEM-RecurDyn simulation model was validated through field experiments. This model provides a novel approach for investigating the mechanism of complex variable-amplitude screening. The findings offer valuable insights for optimizing the structural design and manufacturing of variable-amplitude vibrating screens.

Credit Authorship Contribution Statement: Jinming Hu: Conceptualization, Investigation, Visualization, Formal analysis, Methodology, Validation, Funding, Writing - original draft. Mei Yang: Conceptualization, Methodology, Data curation, Writing - review & editing, Qianglin Zhang: Investigation, Methodology. Jinfa Yang: Conceptualization, Data curation. Wuyun Zhao: Conceptualization, Methodology, Data curation, Supervision, Writing - review & editing. Yang Bi: Conceptualization, Methodology, Data curation, Supervision, Writing - review & editing.

Acknowledgments: This work was supported by a grant from the National Natural Science Foundation of China (52065006). The authors would like to thank the editor and reviewers of the manuscript for their thoughtful and helpful comments.

References

1. Dong, K.; Yu, A. Numerical simulation of the particle flow and sieving behaviour on sieve bend/low head screen combination, *Miner Eng*, 31 (2012) 2-9. https://doi.org/10.1016/j.mineng.2011.10.020
2. Li, J.; C. Webb, S.S. Pandiella, G.M. Campbell, A numerical simulation of separation of crop seeds by screening-effect of particle bed depth, *Food and Bioprod Process*, 80 (2002) 109-117. https://doi.org/10.1205/09603080252938744
3. Li, Z.; Tong, X. A study of particles penetration in sieving process on a linear vibration screen, *Int J Coal Sci*, 2 (2015) 299-305. https://doi.org/10.1007/s40789-015-0089-7
4. Wang, L.; Zhang, S.; Cui, T.; Gao, Y.; Wang, B. Kinetic characteristics of a bionic screen with continuous variable amplitude from front to rear and behaviour of maize mixture on the screen, *Powder Technol*, 424 (2023) 118370. https://doi.org/10.1016/j.powtec.2023.118370
5. Zhao, L.; Zhao, Y.; Bao, C.; Hou, Q.; Yu, A. Optimisation of a circularly vibrating screen based on DEM simulation and Taguchi orthogonal experimental design, *Powder Technol*, 310 (2017) 307-317. https://doi.org/10.1016/j.powtec.2017.01.049
6. Jiang, H.; Zhao, Y.; Duan, C.; Yang, X.; Liu, C.; Wu, J.; Qiao, J.; Diao, H. Kinematics of variable-amplitude screen and analysis of particle behavior during the process of coal screening, *Powder Technol*, 306 (2017) 88-95. https://doi.org/10.1016/j.powtec.2016.10.076
7. Jiang H.; Zhao Y.; Duan C.; Liu C.; Wu, J.; Diao, H.; Qiao, J. Dynamic characteristics of an equal-thickness screen with a variable amplitude and screening analysis, *Powder Technol*, 311 (2017) 239-246. https://doi.org/10.1016/j.powtec.2017.01.022
8. Chen, Y.; S.S. Hsiau, H.Y. Lee, Y.P. Chyou, C.J. Hsu, Size separation of particulates in a trommel screen system, *Chem. Eng. Process. Process Intensif.*, 49 (2010) 1214-1221. https://doi.org/10.1016/j.cep.2010.09.003
9. Jiang, H.; Yu, S.; Pan, M.; Duan, C.; Zhao, Y.; Zhou, Z.; Liu, C.; Wu, J.; Song, B. Effect of excitation parameters on motion characteristics and classification performance of rigid-flexible coupled elastic screen surface for moist coal, *Adv Powder Technol*, 31 (2020) 1196-1208. https://doi.org/10.1016/j.apt.2019.12.029
10. Dong, K.; Wang, B.; Yu, A. Modeling of particle flow and sieving behavior on a vibrating screen: from discrete particle simulation to process performance prediction, *Ind Eng Chem Res*, 52 (2013) 11333-11343. https://doi.org/10.1021/ie3034637

 doi:10.20944/preprints202605.1586.v1

11. Jiang, H.; Qiao, J.; Zhou, Z.; Zhao, Y.; Yang, Y.; Duan, C.; Luo, Z.; Cai, L.; Wang, S.; Pan, M. Time evolution of kinematic characteristics of variable-amplitude equal-thickness screen and material distribution during screening process, *Powder Technol*, 336 (2018) 350-359. https://doi.org/10.1016/j.powtec.2018.06.003
12. Zhao, L.; Zhao, Y.; Bao, C.; Hou, Q.; Yu, A. Laboratory-scale validation of a DEM model of screening processes with circular vibration, *Powder Technol*, 303 (2016) 269-277. https://doi.org/10.1016/j.powtec.2016.09.034
13. Jiang, H.; Duan, C.; Wu, J.; Zhao, Y.; Liu, C.; Luo, Z.; Dong, L.; Zhang, B.; Wang, Z.; Zhang, C.; Yu, X. Kinematics characteristics of the vibrating screen with rigid-flexible screen rod and the behavior of moist coal particles during the dry deep screening process, *Powder Technol*, 319 (2017) 92-101. https://doi.org/10.1016/j.powtec.2017.06.036
14. Wang, L.; Yu, Y.; Zhang, S.; Feng, L.; Song, L. Bionic design and performance test of maize grain cleaning screen through earthworm motion characteristics, *Int J Agric Biol Eng*, 14 (2021) 12-21. https://doi.org/10.25165/j.ijabe.20211403.6534
15. Guo, N.; W.; Huang, J.; Lin, Y. Kinematical Simulation and Analysis of the Combining Vibrating Screen, *Adv Mater Res*, 308 (2011) 2334-2339. https://doi.org/10.4028/www.scientific.net/amr.308-310.2334
16. Wang, L.; Ding, Z.; Meng, S.; Zhao, H.; Song, H. Kinematics and dynamics of a particle on a non-simple harmonic vibrating screen, *Particuology*, 32 (2017) 167-177. https://doi.org/10.1016/j.partic.2016.11.002
17. P.A. Cundall, O.D.L. A discrete numerical model for granual assemblies, *Geotechnique*, 29 (1979) 47-65. https://doi.org/10.1680/geot.1979.29.1.47
18. F. Elskamp, H. Kruggel-Emden, M. Hennig, U. Teipel, Discrete element investigation of process models for batch screening under altered operational conditions, *Powder Technol*, 301 (2016) 78-95. https://doi.org/10.1016/j.powtec.2016.05.039
19. Ning, S.; Xiao, J.; Wang, G.; Huang, P. Study on the particle stratification and penetration of a swing vibrating screen by using DEM, *Eng Computation*, 37 (2020) 881-894. https://doi.org/10.1108/ec-11-2018-0528
20. Ma, Z.; Li, Y.; Xu, L; Discrete-element method simulation of agricultural particles' motion in variable-amplitude screen box, *Comput Electron Agr*, 118 (2015) 92-99. https://doi.org/10.1016/j.compag.2015.08.030
21. Li, Y.; Zhao, P.; Mo, L.; Ren, T.; Zhang, M. Numerical simulation of particle screening efficiency of large multi-layer vibrating screen based on discrete element method, *P I Mech Eng E-J Pro*, 236 (2022) 565-574. https://doi.org/10.1177/09544089211060601
22. Delaney, G.; P.W. Cleary, M. Hilden, R.D. Morrison, Testing the validity of the spherical DEM model in simulating real granular screening processes, *Chem Eng Sci*, 68 (2012) 215-226. https://doi.org/10.1016/j.ces.2011.09.029
23. Xu, G.; Fang, H.; Song, Y.; Du, W. Optimal design and analysis of cavitating law for well-cellar cavitating mechanism based on MBD-DEM bidirectional coupling model, *Agriculture*, 13 (2023) 142. https://doi.org/10.3390/agriculture13010142
24. Wang, X.; Yang, S.; Li, W.; Wang, Y. Vibratory finishing co-simulation based on ADAMS-EDEM with experimental validation, *Int J Adv Manuf Technol*, 96 (2018) 1175-1185. https://doi.org/10.1007/s00170-018-1639-0
25. Dong, K.; Yu, A.;. I. Brake, DEM simulation of particle flow on a multi-deck banana screen, *Minerals Engineering*, 22 (2009) 910-920. https://doi.org/10.1016/j.mineng.2009.03.021
26. Wu, B.; Zhang, X.; Niu, L.; Xiong, X.; Dong, Z.; Tang, J. Research on sieving performance of flip-flow screen using two-way particles-screen panels coupling strategy, *IEEE Access*, 7 (2019) 124461-124473. https://doi.org/10.1109/access.2019.2938847
27. Ma, Z.; Li, Y.; Xu, L.; Chen, J.; Zhao, Z.; Tang, Z. Dispersion and migration of agricultural particles in a variable-amplitude screen box based on the discrete element method, *Comput Electron Agr*, 142 (2017) 173-180. https://doi.org/10.1016/j.compag.2017.08.030
28. Jiang, H.; Zhao, Y.; Qiao, J.; Duan, C.; Chen, Z.; Zhou, E.; Diao, H.; Zheng, D. Process analysis and operational parameter optimization of a variable amplitude screen for coal classification, *Fuel*, 194 (2017) 329-338. https://doi.org/10.1016/j.fuel.2016.12.091
29. Jiang, H.; Qiao, J.; Zhao, Y.; Duan,C.; Luo, Z.; Liu, C.; Yang, Y.; He, J.; Zhao, L.; Pan, M. Evolution process and regulation of particle kinematics and spatial distribution driven by exciting parameters during

 doi:10.20944/preprints202605.1586.v1

variable-amplitude screening, *Powder Technol*, 330 (2018) 292-303. https://doi.org/10.1016/j.powtec.2018.02.028

30. Chen,Y.; Cheng,Y.; Chen, J.; Zheng, Z.; Hu, C.; Cao, J.; Design and experiment of the buckwheat hill-drop planter hole forming device, *Agriculture*, 11 (2021) 1085. https://doi.org/10.3390/agriculture11111085
31. R.D. Mindlin, H. Deresiewicz, Elastic Spheres in Contact Under Varying Oblique Forces, J. appl. mech, 20 (1953) 327-344. https://doi.org/10.1115/1.4010702
32. Y. Tsuji, T. Tanaka, T. Ishida, Lagrangian numerical simulation of plug flow of cohesionless particles in a horizontal pipe, *Powder Technol*, 71 (1992) 239-250. https://doi.org/10.1016/0032-5910(92)88030-l
33. F. Elskamp, H. Kruggel-Emden, Review and benchmarking of process models for batch screening based on discrete element simulations, *Adv Powder Technol*, 26 (2015) 679-697. https://doi.org/10.1016/j.apt.2014.11.001
34. H. Kruggel-Emden, E. Simsek, S. Rickelt, S. Wirtz, V. Scherer, Review and extension of normal force models for the Discrete Element Method, *Powder Technol*, 171.3 (2007) 157-153. https://doi.org/10.1016/j.powtec.2006.10.004
35. A.D. Renzo, F.P.D. Maio, Comparison of contact-force models for the simulation of collisions in DEM-based granular flow codes, *Chem Eng Sci*, 59 (2004) 525-541. https://doi.org/10.1016/j.ces.2003.09.037
36. Qiao, J.; Duan, C.; Jiang, H.; Zhao, Y.; Chen, W.; Huang, L.; Wen, P., Wu, J. Research on screening mechanism and parameters optimization of equal thickness screen with variable amplitude based on DEM simulation, *Powder Technol*, 331 (2018) 296-309. https://doi.org/10.1016/j.powtec.2018.03.031
37. Xiao, J.; Tong, X. Characteristics and efficiency of a new vibrating screen with a swing trace, *Particuology*, 11 (2013) 601-606. https://doi.org/10.1016/j.partic.2012.07.014
38. Li, Z.; Tong, X.; Zhou, B.; Wang, X. Modeling and parameter optimization for the design of vibrating screens, *Miner Eng*, 83 (2015) 149-155. https://doi.org/10.1016/j.mineng.2015.07.009
39. Yin, Z.; Zhang, H. Simulation of particle flow on an elliptical vibrating screen using the discrete element method, Powder Technol, *Powder Technology*, 302 (2016) 443-454. https://doi.org/10.1016/j.powtec.2016.08.061
40. Li, M.; Hu, J.; Yang, M.; Yang, J.; Zhang, Q.; Zubarev, Y.A.; Zhao, W.; Bi, Y. Quality Attributes and Dielectric Properties of Sea Buckthorn Berries under Differing Freezing Regimes and Their Interrelationships. *Foods*, 2022, 11, 3825. https://doi.org/10.3390/foods11233825